Check for updates

Subband Decomposition Based Output-Only Modal Analysis

Dalton L. Stein
Nonlinear Dynamics Laboratory, Fascitelli Center for Advanced Engineering 260, University of Rhode Island, Kingston, RI 02881
e-mail: daltonstein98@uri.edu

He-Wen-Xuan Li[1]
Nonlinear Dynamics Laboratory, Fascitelli Center for Advanced Engineering 260, University of Rhode Island, Kingston, RI 02881
e-mail: hewenxuan_li@uri.edu

David Chelidze
Nonlinear Dynamics Laboratory, Fascitelli Center for Advanced Engineering 260, University of Rhode Island, Kingston, RI 02881
e-mail: chelidze@uri.edu

Output-only modal analysis (OMA) is an indispensable alternative to experimental modal analysis for engineering structures while in operation. Conventional OMA often fails to identify the underlying modal structure with insufficient modal energy contribution. Such low modal participation is expected when the sampled response is subjected to sensor nonlinearity or when specific modes are not directly excited. A novel subband decomposition (SBD) method that resolves modal parameters even with biased modal energy distribution is proposed. It isolates the system response within a narrow frequency subband through a finite impulse response analysis filter bank. Whenever the filter subband captures a resonance, the filtered system response is close-to-singular and contains mainly the resonant mode contribution. A modal cluster metric is defined to identify the resonant normal modes automatically. The modal parameters are also identified and extracted within the subband possessing the locally maximal clustering measure. The proposed method assumes no a priori knowledge of the structure under operation other than the system should have any repeated natural frequencies. Therefore, the SBD algorithm is entirely data-driven and requires minimal user intervention. To illustrate the concept and the accuracy of the proposed SBD, numerical experiments of a linear cantilevered beam with various stationary and non-stationary loading are conducted and compared to other OMA methods. Furthermore, physical experiments on an aluminum cantilever beam examine the method's applicability in field modal testing. Compared to traditional OMA methods, the numerical and physical experiments show orders of magnitude improvement in modal identification error using the proposed SBD. [DOI: 10.1115/1.4055135]

Keywords: output-only modal analysis, subband decomposition, filter banks, non-stationary excitation, linear normal mode

1 Introduction

Modal analysis is a well-adopted engineering practice for structural design and the dynamic characterization of engineering structures. Knowing the modal parameters during the design prevents catastrophic failures due to resonant deformations of structures, reduces excessive wear of machinery components, and mitigates harm to whoever operates the machines. Moreover, the obtained modal model helps explore structural responses to various loading scenarios and guides the structural-model-order reduction.

Modal testing resolves modal parameters (i.e., natural frequencies, modal damping ratios, and mode shapes) using experimentally obtained system responses. Experimental modal analysis (EMA) is a well-established engineering practice to identify modal parameters using both the system's input and output measurements. Typically, the artificial excitation is an impulse force via a modally tuned hammer or a known excitation force provided by shakers. Frequency response functions are estimated based on the obtained modal testing data sets, and frequency domain modal models can be fit to the estimated functions to identify the poles and the modal matrix of the structure. The most frequently used modal parameter identification methods include the peak picking method [1,2], the least square complex exponential method [3], and the least square orthogonal rational function (LSRF) method [4].

In general, EMA is almost only applicable during the design stage of the structure; otherwise, it will impose unnecessary downtime when the system is in operation. To tackle modal testing during operation, output-only modal analysis or operational modal analysis (OMA) was established by using only the response data. OMA has received much attention for its use in on-site field measurements and real-time applications such as structural health monitoring and vibration control [5,6]. OMA algorithms can be grouped into the time- and frequency-domain approaches. For the latter, the basic frequency domain or peak picking technique is used to estimate the natural modes and frequencies from the power spectral density matrix of the response measurements [7]. For closely-spaced modes, this method deteriorates, and the results become biased. The frequency domain decomposition (FDD) method compensates for the deficiencies in the basic frequency domain method without losing its simplicity [8]. In addition, the extension of this method improves the modal damping and frequency estimations and automates the peak picking procedure [9]. However, when the resonant peaks in the power spectral density function are contaminated by non-modal interference, the modal parameters cannot be resolved. The Ibrahim time domain and eigen system realization algorithm (ERA) [10] developed in the 1970s and 1980s are widely used time-domain algorithms. However, these methods assume that the system is excited by either white Gaussian noise or an impulse (including a free-response case). The general realization algorithm extends the ERA method to allow for modal parameter estimation for arbitrarily excited systems. However, it uses the input signal to construct a weighted Hankel matrix, rendering it an EMA method [11].

It is also well recognized that the OMA-resolved modal parameters are primarily affected by the mass distribution of the structure (i.e., we experience mass scaling of the mode shapes) and the extraneously low modal participation usually caused by excitation and observer biases. Such biases affect the use of the OMA methods that directly exploit the covariance/correlation matrices of the response data. A well-known example is the proper orthogonal decomposition (POD) which uses the singular value decomposition (SVD) of the response matrix [12] as a solution. Although widely used for modal identification, it is only suited for systems with uniform mass distribution. Otherwise, the corresponding non-uniform mass matrix must be known a priori to accurately estimate the linear normal modes (LNM) from the raw time series, which is impractical for complicated mechanical systems. This

[1]Corresponding author.

Contributed by the Technical Committee on Vibration and Sound of ASME for publication in the Journal of Vibration and Acoustics. Manuscript received March 12, 2022; final manuscript received July 25, 2022; published online August 24, 2022. Assoc. Editor: Melih Eriten.

 Copyright © 2022 by ASME

Downloaded from http://asmedigitalcollection.asme.org/vibrationacoustics/article-pdf/145/1/011005/6912201/vib_145_1_011005.pdf by guest on 15 October 2024

problem is resolved by the smooth orthogonal decomposition (SOD) using the generalized singular value decomposition (GSVD) to find a set of smooth orthogonal temporal coordinates of the sampled response data [13]. The SOD could accurately estimate an undamped system's LNMs and natural frequencies without knowing the mass matrix. However, when the system under investigation is in operation, not all the LNMs are necessarily excited. The operation-biased system response impairs the modal identification quality when the decomposition is solely based on the observed energy (e.g., the covariance matrix). Therefore, energy-based OMA methods like the POD and SOD tend to fail when the observation is biased by the sensors themselves or by extraneous non-system events. This can be caused by biased sensing, localized electrical noise, and unexpected intermittent events in real-world scenarios. As a result, essential modal information cannot be directly extracted from the system response. Hence, there is a need for a new method to accommodate the deficiencies experienced in POD and SOD while preserving the simplicity of the algorithms.

Some early work tried to resolve the biased modal energy problems by isolating the modal identification process within a small frequency bandwidth. One method designs bandpass filters to isolate individual modes allowing the successful extraction of LNMs in structures with non-uniform mass distribution using POD [14]. The time domain decomposition uses similar ideas in which digital bandpass filters were designed to isolate a system's responses, where each behaves like a single-degree-of-freedom system [15]. However, both proposed methods require user input to design the filters for each mode in the response data and require users' judgment on where the modal frequency is located. Recently, filter banks have been applied in structural health monitoring and fault diagnosis for mechanical systems [16]. However, to the author's best knowledge, no study has explored using filter bank structures to assist modal parameter identification.

This paper aims to isolate and identify modal structures located at or near resonance frequencies where the dynamics of the system are known to be singular (i.e., the system response is composed of or dominated by only one mode). In this new method, the total bandwidth of the response is partitioned into predetermined subbands via a uniform analysis filter bank. Afterward, the SOD is applied to each subband to resolve the underlying low-rank modal structure. Unlike the SVD applied in time domain decomposition, the basis found from SOD is generally not orthogonal. For bandlimited signals at a resonant frequency, the response should be dominated by only one mode, and one should expect the matrix of modes obtained by SOD to be close to rank deficient. By exploiting this property of SOD, resonance peaks and modal structures can be identified using a classification criterion to find the close-to-singular modal structures within the subbands. To justify the advantages of the proposed method, numerical and physical experiments will be conducted to emulate the excitation bias resulting from the limited bandwidth of the environmental loading (e.g., non-white Gaussian loading) or the operational loading correlated to the system response (e.g., harmonic excitation) and the observer bias due to sensor nonlinearity for specific frequency range(s).

The remainder of the paper is arranged as follows: Sec. 2 provides a brief overview of the preliminaries, particularly the POD and SOD algorithms, and directs the readers to the relevant literature for further details; Sec. 3 formulates the proposed methodology; Sec. 4 presents numerical and experimental examples are explored to compare the newly proposed methodology and some popular OMA methods; afterward, a thorough discussion and important remarks are followed by the cConclusions.

2 Popular Output-Only Modal Analysis Methods and Their Limitations

For a given vibratory mechanical system, its dynamics—when subjected to a small perturbation—can be assumed to be a linear combination (i.e., superposition) of a set of time-invariant spatial functions and their corresponding time coordinates. Therefore, one looks for such coherent spatiotemporal structures through the separation of variables. In practice, this separation of variables is conducted by decomposing a matrix that contains a sample of the underlying continuous field of the structural response in time. As a result, we consider a sampled scalar field in the form of a data matrix $X \in \mathbb{R}^{m\times p}$ for m time snapshots of position, velocity, or acceleration measurements at p distinct spatial points. Since no input information is directly given, for almost all output-only modal analysis methods, spatiotemporal dynamics separation is realized by investigating the correlation between the acquired system response and the transformed version of the correlation matrix (e.g., power spectral density estimates in FDD). The POD, the SOD, and the ERA are considered as examples to illustrate the limitations of some standard output-only modal analysis methods and show the necessity and advantage of the proposed modal analysis framework. These methods are widely recognized in OMA, are easy to implement, and do not require special processing of the data (e.g., transformation into frequency domain).

2.1 Proper Orthogonal Decomposition. POD resolves the underlying spatiotemporal structure of the system dynamics by separating the field into a linear combination of spatially and temporally independent basis function pairs, where both the spatial and the temporal basis functions are orthogonal (or orthonormal) [17,18]. The basis is chosen in such a way that each successive lower-dimensional representation of the original field provides the best possible approximation in the least squares sense. The POD problem can be solved by the eigenvalue problem of the sample-correlation matrix [12]. However, the most practical implementation is obtained by performing an SVD on the trajectory matrix, X, i.e.,

$$X = U\Sigma V^T \tag{1}$$

where the columns of orthonormal U are the proper orthogonal coordinates, $\Sigma = \mathrm{diag}(\sigma_i)$ is a diagonal matrix where the square of the- diagonal elements, $\lambda_i = \sigma_i^2$, are the proper orthogonal values, and the columns of orthonormal V are the proper orthogonal modes (POMs). It is important to note that the λ's are ordered based on modal energy content, i.e., $\lambda_1 \geq \lambda_2 \geq, \ldots, \geq \lambda_p$. In the context of modal analysis, the most energetic mode in a given experiment or simulation will have the largest λ. Therefore, the energy (or the variance) of data dictates the resolved spatial functions (modes) and the temporal functions (temporal coordinates); as a result, the modal participation affects the ability and accuracy of the resolved proper orthogonal modes from a given data set [12].

2.2 Smooth Orthogonal Decomposition. The idea behind the SOD is to find a smoothest lower-dimensional approximation of a sampled scalar field by minimizing the roughness in the associated time coordinates. In other words, SOD finds a set of basis vectors, Φ, where a projection of the original data matrix onto this basis arranges the time coordinates according to their maximal smoothness [13] while keeping their variances the same. The degree of smoothness of each time coordinate is described by the variance of the corresponding time derivative approximated by some finite difference operator, $\mathcal{D}$. The SOD problem is solved by performing a generalized singular value decomposition (GSVD) on the matrix pair X and $\dot{X}$, where $\dot{X} = \mathcal{D}X$

$$X = UC\Phi^T \text{ and } \dot{X} = VS\Phi^T \tag{2}$$

where $U \in \mathbb{R}^{m\times p}$ and $V \in \mathbb{R}^{m\times p}$ are matrices with orthonormal columns, $C = \mathrm{diag}(c_i) \in \mathbb{R}^{p\times p}$ and $S = \mathrm{diag}(s_i) \in \mathbb{R}^{p\times p}$ are diagonal matrices, and the common spatial basis of the decomposition, $\Phi \in \mathbb{R}^{p\times p}$ are the *smooth modes* (SMs). The SMs are invertible when X is full-rank [19,20] (but not necessarily orthogonal), and their corresponding temporal coordinates in UC are called the smooth orthogonal coordinates (SOCs). The SOCs are conventionally

Downloaded from http://asmedigitalcollection.asme.org/vibrationacoustics/article-pdf/145/1/011005/6912201/vib_145_1_011005.pdf by guest on 15 October 2024

sorted according to their "smoothness," characterized by $\mu_i = c_i^2/s_i^2$ smooth values. SOD resolved modes are both energetic and smooth. Therefore, the low-participation modes are more likely to be resolved as long as they are smoother than the more energetic modes or noise.

2.3 Eigensystem Realization Algorithm. In POD and SOD analysis, only the auto-correlation (or auto-covariance) matrices are involved. Other OMA methods utilize the cross-correlation from two temporally-correlated matrices [21–23]. The ERA is a well-recognized example of such a method [24]. Originating from the control theory of linear systems, ERA solves for the system dynamics (or modal parameters) by assuming the system response is either free decay or under wide-band spatially-uncorrelated random excitation. The system response in the state-space form is assumed to be an observation of a system dynamics described by a system matrix A and an initial state u_0,

$$y(n) = OD^n u_0 \tag{3}$$

where O is the observation matrix and $Du_0 = \exp(\mathcal{A}\Delta t)u_0$ is the solution to the underlying linear time-invariant first-order system $\dot{u} = \mathcal{A}u$ with initial condition u_0. The algorithm of ERA, in general, considers an ensemble of system responses $Y(n) = [y_1(n), y_2(n), \ldots]$ evaluated at the sample time n and their corresponding initial conditions $U_0 = [u_{01}, u_{02}, \ldots]$; where the following relationship holds,

$$Y(n) = OD^n U_0 \tag{4}$$

when only one data set is involved, the ensemble equation Eq. (4) reduces to Eq. (3). Based on the ensemble data matrix Y, two Hankel matrices that are one sample time away from each other are created and decomposed as follows [10,22],

$$H(1) = \begin{bmatrix} Y(0) & Y(1) & \cdots \\ Y(1) & Y(2) & \cdots \\ \vdots & \vdots & \ddots \end{bmatrix} = PQ \tag{5}$$

$$H(2) = \begin{bmatrix} Y(1) & Y(2) & \cdots \\ Y(2) & Y(3) & \cdots \\ \vdots & \vdots & \ddots \end{bmatrix} = PDQ$$

where $P = [O, OD, OD^2, \ldots]^T$ is the observability matrix and $Q = [U_0, DU_0, D^2U_0, \ldots]$ is the controllability matrix. The unbiased estimates of P and Q are usually obtained through the SVD of $H(0) = U_{H_0}\Sigma_{H_0}V_{H_0}^T$ and by letting $\hat{P} = U_{H_0 r}\Sigma_{H_0 r}^{1/2}$ and $\hat{Q} = \Sigma_{H_0 r}^{1/2}V_{H_0 r}^T$, respectively [24,25]. Then, the estimated system dynamics can be obtained as

$$\hat{D} = \hat{P}^{\dagger}H(1)\hat{Q}^{\dagger} \approx \Sigma_{H_0 r}^{-1/2}U_{H_0 r}^T H(1) V_{H_0 r}\Sigma_{H_0 r}^{-1/2} \tag{6}$$

with $(\cdot)^{\dagger}$ being the Moore-Penrose pseudo-inverse, and r is the order of realizations of the system matrix (where $r/2$ is the number of modes considered in the above full-rank decomposition). Then, the eigen decomposition to the estimated r-realization system dynamic matrix can be accomplished via [24,25]

$$\hat{D} = \Psi' \Omega \Psi'^{-1} \tag{7}$$

and the system poles are resolved via $\hat{p}_i = \ln(\omega_i)/\Delta t$ and the mode shapes in the physical space are derived as $\Psi = \hat{P}\,\Psi'$. The ERA assumes the responses of the considered system are free decays, and it tries to obtain the system dynamics $\hat{D}$ through averaging over many trials; as a result, the estimated system dynamics are easily affected by the applied load, especially when it is non-stationary.

Although widely adopted in the contemporary OMA, the aforementioned methods may fail to extract the modal parameters when there is low modal participation, observer-biased modal energy distribution, or energy leakage from non-impact excitation. For example, if one of the modal structures is not properly excited during the recording and its energy contribution to the overall system response is far less than other modes, the POD may completely fail to extract this mode. Even though smooth orthogonal decomposition was proposed to resolve non-orthogonal modes by rendering the resolved temporal basis functions (temporal coordinates) to be maximally smooth, it may still suffer from the above-mentioned issues. Numerical examples will be illustrated in regard to these problems in Sec. 4.

3 The Proposed Subband Decomposition Algorithm

The idea behind the subband decomposition (SBD) algorithm is to isolate the modal structure within a certain frequency range that is close to a resonant frequency. When at the damped natural frequency, the system's frequency response function is expected to be close to singular (and it is singular when there is no damping) and the system response is dominated by the mode associated with that resonant frequency [24,26]. Past research has used filter theory to isolate these modal structures but relies on the user to manually locate the resonances in the frequency domain beforehand [14,15]. This section proposes an algorithm to partition the vibrational bandwidth into many subbands and identify the subbands containing singular modal structures based on a new and robust criterion.

The new criterion uses and exploits the essential property of the SOD to extract the close-to-singular system dynamics, which corresponds to the underlying mode shape of the linear mechanical system and the associated modal frequency. We assume the system dynamics can be decomposed into the following pole residue form

$$H(j\omega) = \sum_{l=1}^{\infty}\left(\frac{R_l}{j\omega - p_l} + \frac{R_l^*}{j\omega - p_l^*}\right) \tag{8}$$

where the modal parameters are embedded in the residue matrices R_l and the poles $p_l = j\omega_{dl}$; and $(\cdot)^*$ denotes the complex conjugation. This assumption implies that whenever the system response is close to a resonant frequency [13], the resolved system dynamics is composed of close to only one modal structure and its corresponding damped natural frequency by assuming no closely-spaced modes are present.

If a set of collected spatiotemporal response data X is filtered to present only in a limited bandwidth, such filtered response Y_i in the frequency domain can be treated as a linear combination of a limited number of frequency components (ideally, only one frequency component), each of which shares modal contribution from all the modes present in this limited bandwidth. Whenever the subband approaches a resonance, the contribution from that resonance dominates the current filtered data set. By applying the SOD to the subband system response matrix Y_i which is centered at a resonant frequency, the SOD will identify mode shapes that are similar to each other; in other words, the resolved SMs will span a closely-spaced modal subspace (if not lying on the same modal subspace when there is no noise and only one mode is active).

3.1 Finite Impulse Response Bandpass Filter Design. Ideally, the proposed method decomposes the obtained system response data into a sum of bandpass-filtered response matrices without energy leakage. Therefore, a proper digital bandpass filter must approximate the ideal filter. The filter design has to isolate the frequency component of the response data so that when the center frequency of the bandpass filter approaches the resonance, close-to-singular system dynamics can be identified by the SOD. Although a direct application of bandpass filtering in the frequency domain (e.g., using the fast Fourier transform) may be used, in the proposed algorithm, a filter bank is designed before the subband

Downloaded from http://asmedigitalcollection.asme.org/vibrationacoustics/article-pdf/145/1/011005/6912201/vib_145_1_011005.pdf by guest on 15 October 2024

decomposition without explicitly transforming the response data between time and frequency domain to reduce the computational overhead. The narrow-band decomposition of the trajectory matrix is conducted in the time domain via convolution by first designing a finite impulse response (FIR) analysis filter bank. An FIR filter bank is preferred due to its balance of stability, linearity, and ease of design.

We consider the impulse response of an ideal bandpass filter given by

$$h_D(n) = \frac{1}{2\pi}\left(\int_{-\omega_2}^{-\omega_1} e^{j\omega n}\mathrm{d}\omega + \int_{\omega_1}^{\omega_2} e^{j\omega n}\mathrm{d}\omega\right) \tag{9}$$

Directly evaluating the integrals results in

$$h_D[n] = \frac{\omega_2}{\pi}\mathrm{sinc}(\omega_2 n) - \frac{\omega_1}{\pi}\mathrm{sinc}(\omega_1 n) \tag{10}$$

where ω_1 and ω_2 are the lower and upper cutoff frequencies of the bandpass filter, respectively. $h_D[n]$ is the discrete-time ideal impulse response of the filter. To obtain the actual filter coefficients, we must multiply $h_D[n]$ by some window function, $w[n]$.

Design criteria for the bandpass filter must be specified to satisfy the requirements of the application. In the case of isolating individual vibration modes, we wish to have a bandpass filter with a very sharp transition width and a stopband attenuation that is lower than the noise floor of the response signal. Here, a Kaiser window is used, which gives us the ability to trade off the transition width against the stopband ripple. A practical filter design approach given in Ref. [27] is used to emphasize important filter parameters used in our application. The stopband attenuation, A, is a function of the passband and stopband ripples, δ_p and δ_s, respectively. This stopband attenuation is found through $A = -20\log_{10}(\delta)$ where $\delta = \min(\delta_s, \delta_p)$. The passband ripple, δ_p, does not have any strict specifications for our application since we are only concerned with rejecting out-of-band modal contributions. Hence, the stopband ripple plays an important role in isolating vibration modes and must be selected to satisfy the stopband attenuation, A. After which, the filter-order, N (i.e., number of coefficients), can be found through $N \geq (A - 7.95)/(14.36\Delta f)$ where Δf is the normalized transition width. The transition width is specified by the user and can be selected to be as "sharp" as needed. Note that a sharp transition width prevents modal contributions at the edge of the bandpass filter from leaking into the subband. The piecewise relationships that govern the Kaiser window are given by [27] and stated below

$$w[n] = \begin{cases} \dfrac{I_0\left(\beta\left[1 - \left(\dfrac{2n}{N-1}\right)^2\right]^{\frac{1}{2}}\right)}{I_0(\beta)}, & \dfrac{-(N-1)}{2} \leq n \leq \dfrac{(N-1)}{2} \\ 0, \quad \text{otherwise} \end{cases} \tag{11}$$

where I_0 is the zero-order modified Bessel function of the first kind and N is the number of filter coefficients needed to satisfy the design parameters. The ripple control parameter is then computed as,

$$\beta = \begin{cases} 0.1102(A - 8.7), & 50 < A \\ 0.5482(A-21)^{0.4} + 0.07886(A-21), & 21 \leq A \leq 50 \\ 0.0 & A < 21 \end{cases} \tag{12}$$

where A is the stopband attenuation. The FIR filter coefficients can then be obtained by multiplying the ideal impulse filter response and the window function,

$$h[n] = h_D[n]w[n] \tag{13}$$

The original trajectory matrix is in the form of a tall-and-skinny matrix with $m \gg p$. Each column in X is convolved with the filter coefficients in Eq. (13) to filter the entire response,

$$Y[m + p - 1, p] = \sum_{k=0}^{N-1} h[k]X[m - k, p] \tag{14}$$

where $Y \in \mathbb{R}^{(m+p-1)\times p}$ is the output of the filtered data matrix X and N is the number of coefficients needed for the proposed filter to satisfy the design specifications.

3.2 Filter Bank Construction and Analysis. We aim to partition the bandwidth of a system response signal into M subbands, where each subband contains a bandlimited spectrum governed by the lower and upper cutoff frequencies (i.e., ω_1 and ω_2) of the M bandpass filters in the array, see Eq. (9). This step determines the quality of the resolved subband SMs, which affects the accuracy of determining the modal structures from the obtained data. To help better conceptualize the proposed subband decomposition algorithm, Fig. 1 visually summarizes the proposed decomposition method.

The raw data is first fed into the pre-designed analysis filter bank and convolved with the M impulse response functions separately. The window function and design criteria remain constant throughout the banks; however, we must slide the passband region over the usable bandwidth,

$$h_i[n] = h_{D_i}[n]w[n] \text{ for } i = 1, 2, \ldots, M \tag{15}$$

where the index i corresponds to the ith passband region for that bandpass filter and $h_i[n]$ corresponds to the FIR filter coefficients of each bandpass filter in the filter bank. An overlap ratio can be specified between adjacent subbands if desired. Then the discrete-time convolution is performed between the data matrix, $X \in \mathbb{R}^{m\times p}$, and the FIR coefficients $h_i[n]$ for each subband,

$$Y_i[m + p - 1, p] = \sum_{k=0}^{N-1} h_i[k]X[m - k, p] \tag{16}$$

The SOD is applied to each bandlimited trajectory subband, Y_i,

$$Y_i = U_i S_i \Phi_i^{\mathrm{T}} \text{ and } \dot{Y}_i = V_i C_i \Phi_i^T \tag{17}$$

The common basis for each bandlimited response, Φ_i, contains the SMs, which are expected to be rank deficient if the subband is centered on a resonant frequency. Only the SM matrices for each subband are stored in the aforementioned procedure. Thus, the algorithm does not have demanding memory requirements. The authors considered a maximum 3×10^4 subbands without any memory storage issues. However, the maximum number of subbands allowed will depend on the user's computer system. The algorithm can be parallelized for accelerated computation for clusters with enough random access memory.

3.3 Subband Cluster Measure for Modal Identification. Since the original trajectory matrix is partitioned into many subbands, it is important to have an automated selection process to identify the resonant subbands. When decomposing a subband that overlaps with a resonant frequency using SOD, the SMs are expected to exhibit similar displacement amplitudes. This obviously assumes minimal leakage of other modes into the subband. The SVD (or POD) does not share this property since the right singular vectors in V have to be orthogonal. Therefore, if one were to apply the POD to the same subband, regardless of whether the subband is centered at a resonant frequency or in between two resonances, the resolved mode shapes would always be orthogonal, and the proposed identification metric will fail. The clustering measure exploits this characteristic of SOD to identify the resonant subbands across the entire partition discussed in Sec. 3.2. The resolved SMs in a resonant subband are expected to be closely-spaced or clustered. Therefore, this clustering of resolved SMs is exploited to identify the underlying modal structure within each subband.

If the identified SMs in Φ_i are highly correlated, the underlying dynamics is close to singular (or rank-1). In contrast, there are no resonant modes whenever the resolved subband SMs are less clustered. Since SOD is less sensitive to the variance of the data, the

Downloaded from http://asmedigitalcollection.asme.org/vibrationacoustics/article-pdf/145/1/011005/6912201/vib_145_1_011005.pdf by guest on 15 October 2024

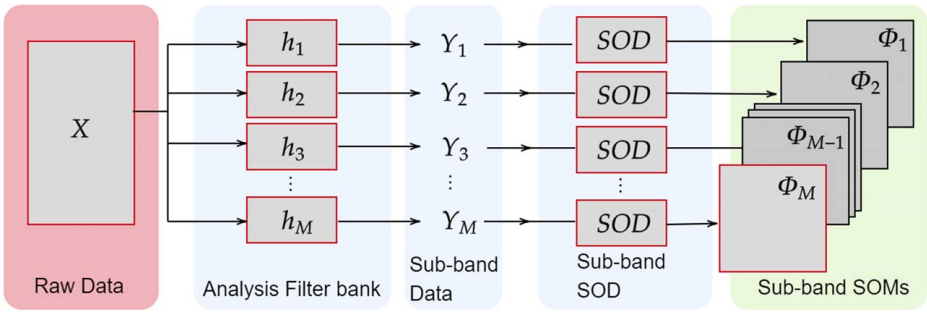

Fig. 1 Graphical illustration of the algorithm to obtain the subband smooth modes Φ_i, $i = 1,2,\ldots, M$ from the raw data matrix X. The raw data X will first be fed into the pre-designed analysis filter banks h_i, $i = 1,2,\ldots, M$ to obtain M m-by-p subband data matrices Y_i; then, all the subband data are input to the same modal decomposition algorithm (i.e., SOD) and the SMs are saved for modal identification in the modal clustering algorithm. The filter bank is predefined, i.e., the filtering and decomposition process for each subband can be conducted in parallel.

subband SOD helps isolate the mode in the current subband by negating the leakage effects due to the highly energetic out-of-band modes.

To characterize the clustering behavior of the subband SMs, a weighted angular similarity between identified SMs in $\Phi \in \mathbb{R}^{p\times p}$ (i.e., column-wise) is considered. Note that this cluster measure is to be computed for $\Phi_i \; \forall \; i = 1, 2, .., M$. First, column-wise cosine similarity is computed

$$\{S_{jk}\}_i = \left| \frac{\phi_j^T \phi_k}{||\phi_j|| ||\phi_k||} \right| \tag{18}$$

where $\|\cdot\|$ denotes the l^2 norm, see Fig. 2(*a*). The absolute value is used to constrain the output between 0 and $\pi/2$ degrees. It is desirable to normalize S_{jk} by $\pi/2$

$$\{\Theta_{jk}\}_i = \frac{2}{\pi}\cos^{-1}(S_{jk}) \tag{19}$$

where $\Theta_{jk} \in \mathbb{R}^{p\times p}$ is a normalized angular similarity matrix whose elements are bounded between zero and one. An element with a similarity of zero corresponds to a pair of orthogonal vectors being compared, while a value of one corresponds to a set of linearly dependent vectors. It is important to note that $\Theta_{jj} = 1$ and

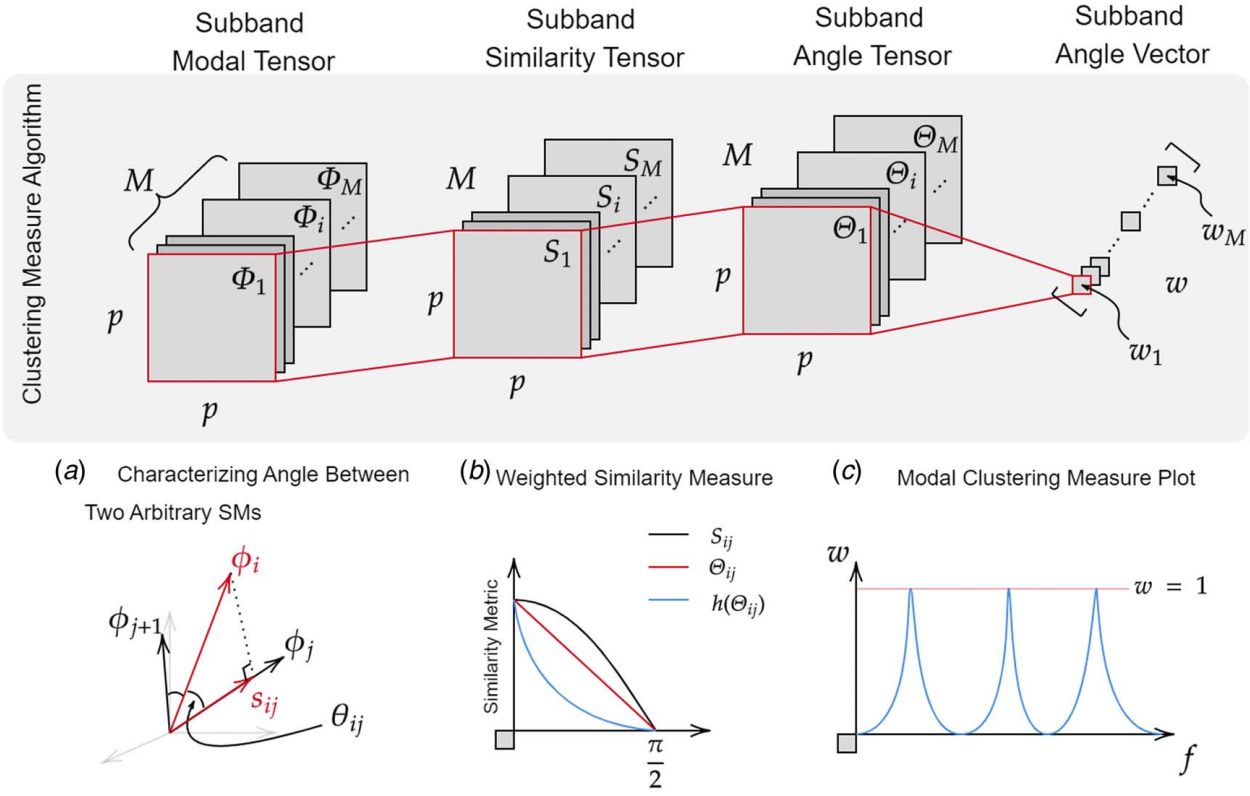

Fig. 2 Graphical illustration of the clustering algorithm. The similarity measures S_i are obtained from the columns of the subband modal matrices (tensors): Φ_i. (*a*) Illustrates the angle between the subband SMs obtained by imposing Eq. (19), which yields a similarity metric that is linearly dependent on the angle between two arbitrary subband SMs, (*b*) illustrates the effect of the difference between S_{jk} and Θ_{jk}, and the effects of adding weights to the similarity metric. The clustering metric w is obtained by summing all elements in matrix $h(\Theta)$ (or Θ if no weight is applied). An ideal case of the similarity metric as a function of frequency is shown in (c) for a bandwidth of interest with three modes.

Downloaded from http://asmedigitalcollection.asme.org/vibrationacoustics/article-pdf/145/1/011005/6912201/vib_145_1_011005.pdf by guest on 15 October 2024

$\Theta_{jk} = \Theta_{kj}$, which is the result of finding the inner product of the same vector. When the SMs are a complete set of orthogonal vectors in the column space, the resultant Θ_{jk} will be the $p \times p$ identity matrix, I_p. Furthermore, when the SMs are all linearly dependent, then the resultant Θ_{jk} will be the $p \times p$ matrix filled with ones, J_p.

To differentiate the subbands encompassing a resonant frequency even further, an exponential function of the form $h(\Theta_{jk}) = a\exp^{-b\Theta_{jk}}$ is used to weight the elements in Θ_{jk}. To use the same scale, the following condition is imposed: $h(0) = 1$, which results in $a = 1$. The parameter b is found from the condition $h(1) = \varepsilon$ for $\varepsilon \ll 1$ and is left for the user to tune in to the post-processing stage if needed.

Transforming the similarity measure S_{ij} to the angle Θ_{ij} provides a linear metric that characterizes the distance between the two SMs within a subband. The imposition of the weight $h(\cdot)$ provides a family of similarity metrics that emphasizes the location of the modal structure by penalizing the similarity exponentially. Figure 2(*b*) shows similarity functions with and without the weighting as the angle between two arbitrary SMs approaches $\pi/2$. For the studies in Sec. 4, we choose $b = 10$ for the weighting function, and for the experimental study in Sec. 5, we choose $b = 5$. This parameter b is what further distinguishes subbands containing a resonance from non-resonance. It is important to note that the weighting will have little effect when all SMs are linearly dependent on a subband. This weighting only affects SM matrices that do not contain a close to singular structure, thus distinguishing the non-resonant subbands from the resonant subbands.

The elements in the matrix Θ_{jk} are then summed together to reduce the classification criterion to a scalar. The maximum of this sum will depend on the number of measurement points used in the study, which is p^2 for p distinct measurement locations. Thus, we propose to divide the sum by p^2, which normalizes the criteria such that the maximum is 1, i.e.,

$$w_i = \left\{ \frac{1}{p^2} \sum_{j=1}^{p} \sum_{k=1}^{p} h\left(\Theta_{jk}\right) \right\}_i \tag{20}$$

where each element in the vector w_i is bounded between

$$\frac{1}{p} \leq w \leq 1 \tag{21}$$

where p is the column dimension of the SM matrix, Φ. The criterion is applied to the SM matrix for every subband. The result is an array of elements, $w_i \; \forall i = 1, 2, \ldots, M$ that quantify the linear dependence (singularity) of the SMs in the effective bandwidth of the response. An ideal w as a function of the frequency (or subband index) for a system with three distinct modes is shown in Fig. 2(*c*). A graphical illustration of obtaining the subband clustering measure is summarized in Fig. 2.

3.4 Linear Normal Mode and Damped Natural Frequency Identification. The index of the maximum values in w_i is directly proportional to the damped natural frequency of the resonance. Those with the largest magnitude correspond to a close-to-singular structure and are identified as resonance subbands. Then, the natural frequency (Hz) information is given as

$$\hat{f}_i = BW \times i - \frac{BW}{2} \tag{22}$$

where BW is the bandwidth of the bandpass filters with units in Hz, and i is the subband index when w is a local maximum. In ideal cases, the subbands corresponding to resonance will have $w_i = p^2$. However, this is seldom the case due to damping and noise in the system. Despite this, the information in the w_i vector indicates where the resonances occur. The corresponding modes are contained in the close-to-singular SM matrix, Φ. Since there are p candidate vectors in Φ, the SVD of $\Phi = U\Sigma V^T$ is performed, and the first column in the left singular vectors, U (i.e., dominant mode shape), is selected as the LNM. Alternatively, we could also average all columns in close-to-singular Φ to estimate the corresponding LNM. For free decay responses, the damping ratios can be obtained from the smooth orthogonal coordinates within each identified resonant subband using standard methods such as the logarithmic decrement. For the forced vibration method, the half-power method could be applied to the FRF of the smooth orthogonal coordinates.

4 Numerical Experiments

In this section, the authors explore the application of the proposed SBD algorithm for numerous situations in which the conventional OMA methodologies usually fail. We consider a uniform cantilever beam that is clamped at $x = 0$ and free at $x = L$. The parameters of the beam are kept identical to the ones used in Ref. [28], where the stiffness is $EI = 1$, the mass per unit length $m = 1$, and a unit length of $L = 1$. A total of ten Euler Bernoulli beam elements are used to construct the system's mass and stiffness matrices, M and K, respectively. A Rayleigh damping model is used in numerical experiments. The damping matrix, C, can be approximated by $C = \alpha_1 M + \alpha_2 K$. The first and tenth modes are given the modal damping ratio of $\zeta_1 = 5.0 \times 10^{-3}$ and $\zeta_{10} = 1 \times 10^{-3}$, respectively. After which, the Rayleigh coefficients are computed to be $\alpha_1 = 5.6 \times 10^{-3}$ and $\alpha_2 = 1.36 \times 10^{-5}$. The natural frequencies and damping ratios of the finite element cantilever beam model are given in Table 1. The prescribed modal damping is aimed to emulate an intrinsic low modal participation scenario. This is a consequence of the exceedingly large modal damping of the first mode, whose damping ratio is at least five times greater than any other mode. As a result, the first mode is expected to have very low energy associated with its modal motion.

A comparison of the proposed SBD, the SOD, and the ERA will proceed with a series of examples. The parameters given in Table 2 will be used to construct the uniform analysis filter bank used for SBD. The filter coefficients obtained from these parameters will be used for each numerical example. We aim to show that a general set of parameters can be used for various problems and not tailored to any particular situation. The estimated mode shapes are normalized in the least squares sense before the errors between the estimated modal vectors and the finite element model

Table 1 Natural frequencies and damping ratios of the finite element model of a cantilever beam

Modal parameters for finite element beam		
Mode #	f_n (Hz)	ζ
1	0.560	0.005
2	3.507	0.000821
3	9.822	0.00058
4	19.261	0.000276
5	31.888	0.000304
6	47.773	0.000383
7	67.028	0.000497
8	89.799	0.000641
9	116.109	0.000813
10	144.340	0.001

Table 2 Filter bank parameters for the uniform cantilever beam

Filter bank parameters				
Bandwidth (Hz)	Stopband attenuation (dB)	Stopband ripple (dB)	Transition width (Hz)	Overlap
0.1	−150	3.1623×10^{-8}	0.001	0

Downloaded from http://asmedigitalcollection.asme.org/vibrationacoustics/article-pdf/145/1/011005/6912201/vib_145_1_011005.pdf by guest on 15 October 2024

Table 3 The RMSE between FEM mode shapes and damped natural frequencies compared with the applied OMA method

RMSE lightly damped cantilever beam								
Mode #	E_ϕ				E_ω			
	SOD	SBD	POD	ERA	SOD	SBD	POD	ERA
1	7.7×10^{-2}	7.2×10^{-4}	1.24×10^{-1}	4.35×10^{-1}	N/A	9.6×10^{-3}	N/A	N/A
2	6.5×10^{-3}	7.0×10^{-4}	2.2×10^{-1}	8.67×10^{-2}	1.4×10^{-1}	4.3×10^{-2}	N/A	2.9×10^{-1}
3	2.9×10^{-3}	1.4×10^{-3}	2.43×10^{-1}	6.4×10^{-3}	6.8×10^{-2}	2.8×10^{-2}	N/A	7.2×10^{-3}
4	5.4×10^{-3}	1.8×10^{-3}	2.16×10^{-1}	3.5×10^{-3}	1.8×10^{-2}	1.1×10^{-2}	N/A	1.5×10^{-4}

(FEM) are computed. The errors are found by computing the root-mean-square error (RMSE) between the estimated LNMs and those from the FEM formulation

$$E=\sqrt{\frac{\sum_{i=1}^{q}(x_i-\hat{x}_i)^2}{q}} \tag{23}$$

where $\hat{x}_i$ is the magnitude of the identified normalized mode shape at a specific spatial point, i, and x_i is the magnitude of the normalized FEM mode shape for the same spatial point; and $q=10$ stands for the total number of nodes considered in this study.

4.1 Cantilever Beam: Impulse Excitation. A single impulse is applied to the first transverse displacement node of the beam. The system's impulse response is recorded for 60 s with a sampling frequency of 1000 Hz. The SOD, POD, ERA, and the proposed SBD methodologies are applied to the response matrix to estimate the LNMs of the structure. For the case of SBD, the filter bank parameters in Table 2 are used to construct the coefficients for each filter in the filter bank. The system response is then convolved with the filter bank using Eq. (16). In this example, the first four modes are identified. The error between the underlying FEM modal structure and natural frequencies is compared to those identified by the algorithms. Table 3 summarizes the error between the estimates of the LNMs and damped natural frequencies with that of the FEM model. The proposed identification criterion and identified first LNM are shown in Fig. 3.

4.2 Cantilever Beam: Single Harmonic Excitation. In certain situations, modal tests cannot be conducted using broadband excitation signals (e.g., a sinusoidal sweep or random signals), especially when the excitation system has limited bandwidth or is generated by an open-loop control (the excitation may not be what is prescribed from the input source). Moreover, in operating reciprocating machinery, harmonic forcing, and environment loading appear simultaneously [25]. In such cases, it is desirable if a narrow-band excitation or a single harmonic excitation can be used for modal identification purposes. Here, a single harmonic excitation is used to excite the base of the cantilever beam model. The excitation is of the form $f_e(t)=A\sin(2\pi ft)$, where different excitation frequencies, f, are chosen to understand the effect on the proposed SBD's identification process (Sec. 3.3). For all cases, the excitation amplitude is set to $A=1$. The system is simulated for 100 s using a sampling frequency of 1000 Hz. The whole time series for each forcing frequency is used in the analysis.

The natural frequencies for the modes corresponding to the ten transverse degrees-of-freedom are between 0 Hz and 150 Hz for the unit parameters. For modal tests in the field, the structure's resonance frequencies may not be known ahead of time, and therefore the selection of an appropriate forcing frequency may not be possible. We consider four different forcing frequencies when $f=[25,\ 75,\ 125,\ \text{and}\ 400]$ Hz. Figure 4 shows the proposed resonant subband identification criterion for each case of forcing frequency. These results demonstrate the forcing frequency has a significant effect on the performance of the criterion. In all cases, no LNMs above the forcing frequency cannot be identified. Moreover, for the 75 Hz and 125 Hz cases, the surrounding LNMs are affected by the forcing frequency. For the 400 Hz harmonic input, the criterion indicates that the first nine modes are clearly identified and are successfully extracted by the algorithm. The estimates for modal vectors and natural frequencies in this section are based on the 400 Hz excitation. Figure 5(*a*) shows the error between the estimated modal vectors for each mode. The combined errors for both the estimated modal vectors and natural frequencies for each methodology are summarized in Table 4.

4.3 Cantilever Beam: Non-Stationary Excitation. In this example, a non-stationary forcing function was considered, particularly a sinusoidal sweep (also known as a chirp signal). Node 1 of the system is excited using a linear chirp signal of the form

$$f_e(t)=A\ \sin\left[2\pi\left(\frac{c}{2}t+f_0\right)t+\phi_0\right] \tag{24}$$

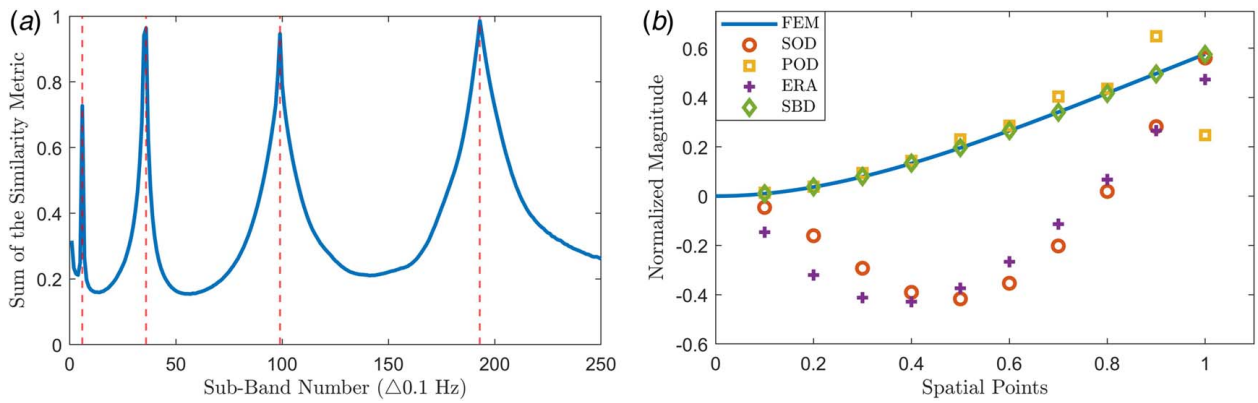

Fig. 3 (*a*) Exponentially weighted angular similarity criterion. The locations of the resonant banks as determined from the FEM model are rendered as dashed vertical lines and (*b*) the first LNM of vibration.

Downloaded from http://asmedigitalcollection.asme.org/vibrationacoustics/article-pdf/145/1/011005/6912201/vib_145_1_011005.pdf by guest on 15 October 2024

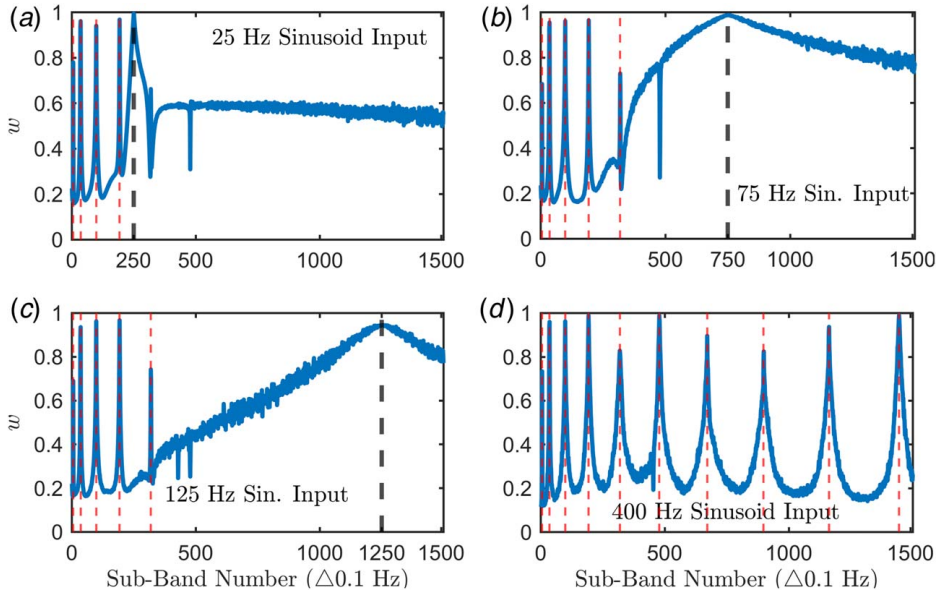

Fig. 4 An exponentially weighted angular similarity measure for: (*a*) 25 Hz sinusoid input, (*b*) 75 Hz sinusoid input, (c) 125 Hz sinusoid input, and (*d*) 400 Hz sinusoid input (continuous curves); the subband location of the forcing frequency is rendered as thick dashed vertical lines for each subplot. The locations of the resonant banks as determined from the FEM model are rendered as thin dashed vertical lines.

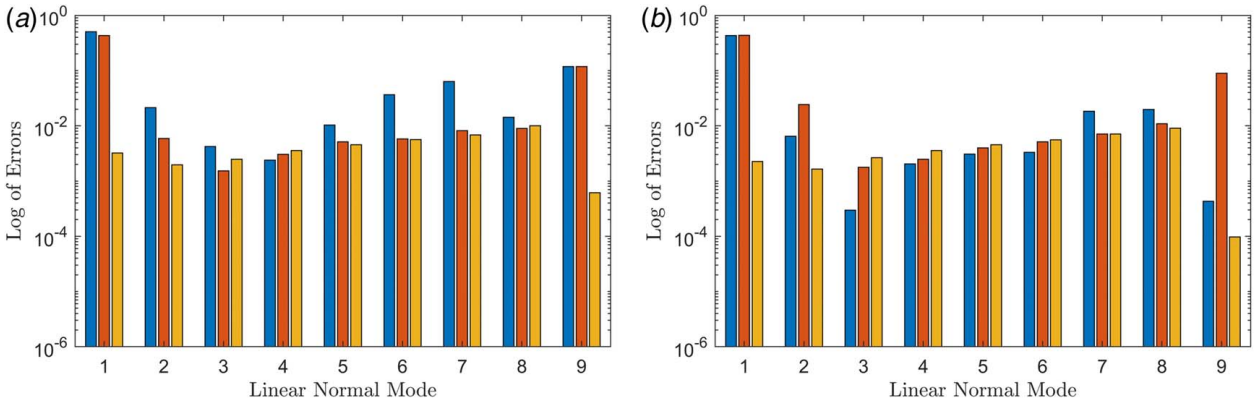

Fig. 5 RMSE of the estimated modes in logarithmic scale for a forced cantilever beam: (*a*) the 400 Hz single harmonic excitation and (*b*) the linear chirp sinusoidal sweep. Illustrated as vertical bar plots from left to right are: Smooth orthogonal decomposition (blue), eigen system realization algorithm (orange), Subband decomposition (yellow).

Table 4 Single harmonic excitation: average of total RMSE between FEM mode shapes and damped natural frequencies compared with the applied OMA method

Average of RMSE under single harmonic excitation						
Mode #	E_ϕ			E_ω		
	SOD	ERA	SBD	SOD	ERA	SBD
All	8.43×10^{-2}	6.26×10^{-2}	4.3×10^{-3}	5.45×10^{-1}	1.43×10^{-1}	2.65×10^{-2}

where A is the forcing amplitude, $c=(f_1-f_0)/T$ is the chirp rate defined by difference between the final frequency, f_1, and starting frequency, f_0, divided by the total sweep time. The phase of the sinusoid is ϕ_0. A simple case of $f_0=0$ and $\phi_0=0$ is considered here. The simulation is sampled at 500 Hz and the input sweeps through the entire effective bandwidth ($0\rightarrow250$ Hz) in $T=100$ s. The sweep rate for this signal is $c=2.5$. The beam is excited by a full sweep through the vibrational signal's entire effective bandwidth (i.e., 250 Hz). Figure 5(*b*) shows the errors computed by Eq. (23) for each mode compared to the FEM LNMs.

5 Experimental Study

An experimental study was performed on a uniform cantilever beam to investigate the effectiveness of the SBD algorithm in an experimental setting. A uniform aluminum beam that is clamped at $x=0$ and free at $x=L$ (assuming cantilever boundary conditions) was considered. The beam dimensions are $610\times25.4\times3.175$ mm. Six accelerometers (PCB U33B42) that are equally spaced across the beam span are used to record the acceleration response of the beam under impulses. The system is excited by an impulse train

Downloaded from http://asmedigitalcollection.asme.org/vibrationacoustics/article-pdf/145/1/011005/6912201/vib_145_1_011005.pdf by guest on 15 October 2024

Table 5 Filter bank parameters for the experimental study

Filter bank parameters for the experimental study				
Bandwidth (Hz)	Stopband attenuation (dB)	Stopband ripple (dB)	Transition width (Hz)	Overlap
0.1	−100	1×10^{-5}	0.05	0

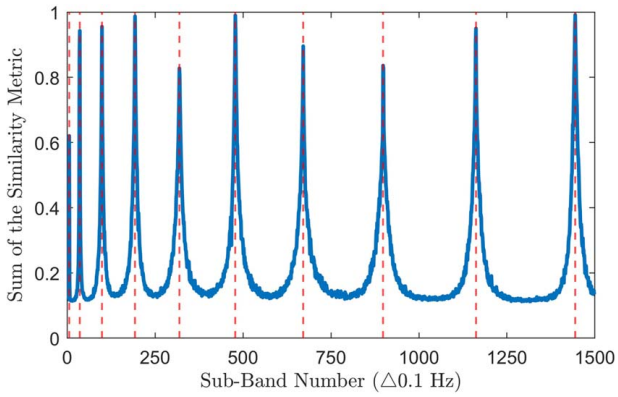

Fig. 6 Weighted angular similarity (continuous curves) for sinusoidal sweep excitation. Resonant frequency bank numbers from FEM (vertical dashed lines).

via a modally tuned hammer (PCB 086C01) across the mid-span of the beam. The roving hammer technique [29] introduces redundancy and more sample responses for averaging when performing modal parameter identification. This guarantees more accurate frequency response function estimates and leads to a more reliable experimental benchmark for comparison.

The results obtained by the LSRF method serve as the benchmark for comparison for the SBD and SOD algorithms, therefore, the identified modes and frequencies using this method are taken as the ground truth. The same procedure is applied to the experimental data from Sec. 4 using the filter bank parameters shown in Table 5. Since only six accelerometers are used during the experiments, a maximum of six modes can be resolved from the obtained data. The sampling frequency is set to 1000 Hz, and an anti-aliasing filter was set to 500 Hz to ensure no higher-order modes or high-frequency noise interferes with the modal parameter identification. The first two modes of the resolved modal structure and identification criterion are shown in Fig. 8.

6 Discussion

The numerical and physical experiments demonstrate the applicability of the SBD algorithm for several practical situations that arise in OMA. The objective of the above studies is to illustrate situations in which the considered conventional OMA algorithms discussed in Sec. 2 fall short of identifying all of the LNMs. The identified shortcomings of the considered OMA algorithms are due to: (1) the excitation-induced low modal participation or (2) the biased response variance introduced by sensor nonlinearity during operational modal testing. The following arguments relating to the considered experiments justify the benefits of the new proposition:

(1) The first numerical example explored the performance of the SOD, POD, ERA, and proposed SBD algorithms by identifying the lower-order LNMs of a cantilever beam for a single impulse applied close to the base. Although the system is lightly damped, both the SOD and ERA still cannot resolve the first mode, which has extraneously low modal participation due to the excitation location. Instead, the identification is biased by the second mode which is observed in Fig. 3. Although the POD appears to identify the first mode better than the SOD and ERA algorithms, the identified mode shape shown in Fig. 3 still does not correspond with the FEM mode shape. Furthermore, the errors for the other three modes are orders of magnitude higher than those identified by the proposed SBD. A train of impulses across the span of the beam may help better excite the first mode for SOD to identify; however, excessive excitation may not always be feasible, especially for large or complicated mechanical systems. Furthermore, the proposed SBD is still expected to work for this situation and therefore has an advantage over the other considered conventional OMA methods.

(2) Two forced vibration examples were considered to understand how the proposed method outperforms others under operational conditions. For the case of single harmonic excitation, the bottom-right subplot in Fig. 4 shows that SBD can accurately identify the first ten modes of the system despite being excited with a high-frequency input signal. SOD and ERA do not share this ability for the first two modes, as shown in Fig. 5. When the frequency is within the bandwidth of the modes of interest, the proposed criteria cannot identify modes higher than the fifth order. This is demonstrated in Fig. 4. In practice, a harmonic excitation with a frequency above the bandwidth of interest (i.e., half of the sampling frequency) can maximize the ability to identify the modes. In this way, all of the modes that are below the effective bandwidth will be appropriately identified. It should be noted that despite the contamination near the excitation band in the criterion shown in Fig. 4 for the 25, 75, and 125 Hz cases, the lower modes are still correctly identified by the criterion. The SBD algorithm generally outperforms both SOD and ERA aside from a few of the identified modes, where only minor differences across the methods can be observed. The ability for SBD to accurately identify the majority of the LNMs using only a single harmonic excitation is valuable for engineering applications where complicated forcing techniques are unavailable or prohibited. Additionally, the proposed

Table 6 Sinusoidal sweep excitation: average of total RMSE between FEM mode shapes and damped natural frequencies compared with the applied OMA method

Average of RMSE under swept-sine excitation						
Mode #	E_ϕ			E_ω		
	SOD	ERA	SBD	SOD	ERA	SBD
All	5.39×10^{-2}	6.42×10^{-2}	4.0×10^{-3}	7.7×10^{-1}	2.3×10^{-1}	3.0×10^{-2}

Downloaded from http://asmedigitalcollection.asme.org/vibrationacoustics/article-pdf/145/1/011005/6912201/vib_145_1_011005.pdf by guest on 15 October 2024

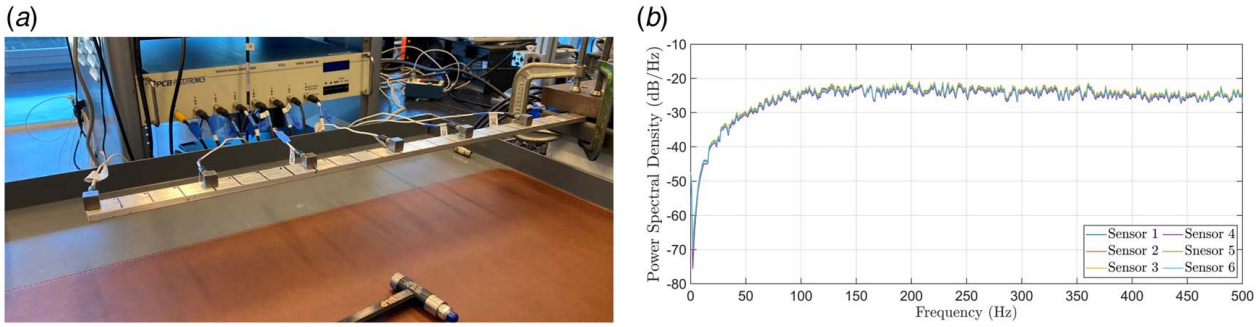

Fig. 7 (*a*) Cantilever beam experimental setup and (*b*) the power spectrum density of the PCB U33B42 accelerometers was subjected to 500 Hz bandwidth white Gaussian noise

Table 7 Identified damped natural frequencies from the experimentally obtained data

Identified natural frequencies f_n (Hz)			
Mode #	EMA-LSRF (Benchmark)	SBD	SOD
1	12.12	12.15	36.62
2	74.86	74.25	81.90
3	210.07	210.45	195.78
4	411.13	408.85	304.75

SBD algorithm provides reliable damped natural frequency estimates, as shown in Table 4.

(3) Being another popular branch of modal testing method, the non-stationary excitation poses challenges to the considered OMA candidates. For ERA, the non-stationarity of the forcing violates its basic assumptions. Regarding SOD, such non-stationarity makes the lower-order modes less energetic; as a result, SOD cannot resolve these modes with extraneously low modal energy. Logarithmic, exponential, or slow linear sweep signals are often employed to overcome this problem; however, the resulting large data set slows down identification significantly. In contrast, the SBD is insensitive to this constraint. As long as an approximately singular modal structure exists in a particular subband, the SBD algorithm can identify it regardless of the type of excitation signal, as shown by the clustering measure in Fig. 6. Figure 5 shows that the proposed SBD has the smallest absolute error attributed to it aside from a few cases from the third to the sixth modes with RMSE shown in Table 6.

(4) The accelerometers used in the experimental hammer tests are biased against lower modes due to their nonlinearity. Fig. 7(*b*) shows the PSD of the accelerometer response

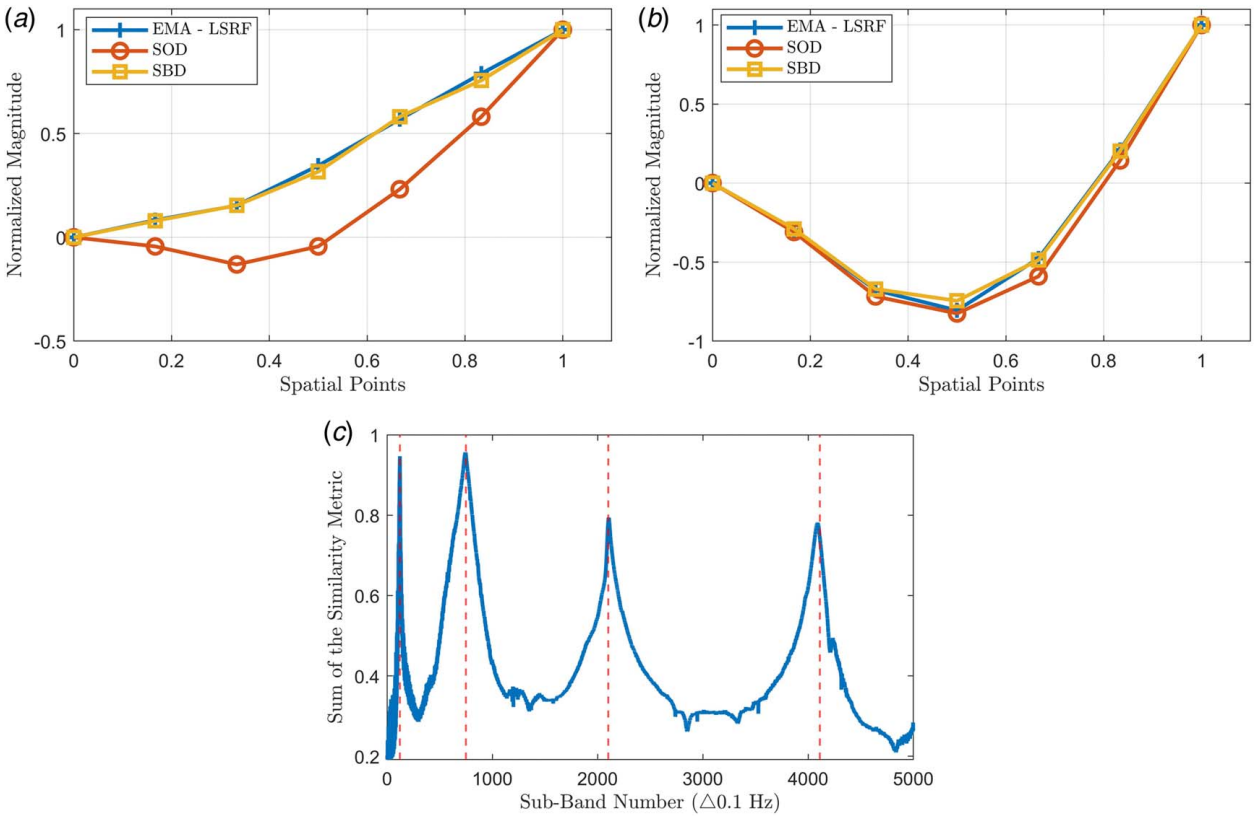

Fig. 8 (*a*) First experimentally identified LNM, (*b*) Second experimentally identified LNM (mode shapes are normalized by the magnitude of the beam tip), and (c) an exponentially weighted angular similarity measure. Vertical dashed lines indicate resonance locations as determined from benchmark EMA-LSRF method.

Downloaded from http://asmedigitalcollection.asme.org/vibrationacoustics/article-pdf/145/1/011005/6912201/vib_145_1_011005.pdf by guest on 15 October 2024

subject to a bandlimited white Gaussian noise (0–500 Hz). The 0–50 Hz region response experiences nonlinear sensor distortion. As a result, LNMs in this region will have lower energy attributed to their modal motion despite being physically energetic (Table 7). Thus, this represents an example of sensor-induced low modal participation for the low-frequency modes. Despite this unfavorable condition, the SBD algorithm can still identify all four modes within range of the results obtained from LSRF, which was used as the ground truth in this example. The same is not valid for SOD, whose first identified mode appears to be a modulation of the first and second actual LNMs of the cantilever beam, as shown in Fig. 8.

7 Conclusion

A novel subband decomposition (SBD) method is proposed to identify modal parameters from response data saddled with low modal participation during operational modal analysis (OMA). This method first decomposes the raw response trajectory matrix into a series of subband response matrices via an FIR uniform analysis filter bank, where each subband matrix is bandlimited. With the in-band frequency-isolated trajectory matrices, the non-orthogonality of the smooth modes (SMs) is exploited to identify the subbands that are close to resonances where the system response is close to singular. This close-to-singular nature of the subband response motivates a new modal clustering measure, developed to robustly identify the resonant subbands without any prior knowledge of the underlying modes. Once the modal frequency or subband is identified, the most-energetic basis of the subspace spanned by the subband SMs is extracted as the corresponding LNM. Compared to various popular OMA methods, SBD successfully identifies the lower energy LNMs even if the subband response is contaminated by energy leakage from the higher-energy out-of-band modes.

Numerical experiments of a cantilever beam are considered to examine the modal identification accuracy of SBD when the collected response is biased by low modal participation under various stationary and non-stationary loading conditions. For identification accuracy, the results show as much as a two-orders-of-magnitude reduction in SBD estimation error compared to the conventional OMA methods. These case studies also validate the applicability and versatility of the proposed SBD in applications that are limited to narrow-band and non-stationary excitation techniques. Furthermore, to validate the applicability of the SBD in modal testing, physical experiments on a cantilever beam are conducted. The experimental results show a significant advantage of the SBD-based identification when low-frequency modes are subject to sensor nonlinearity-induced low modal participation. The experimental results confirm the advantage of the proposed SBD over various popular OMA methods in identifying LNMs with low modal energy.

Conflict of Interest

There are no conflicts of interest.

Data Availability Statement

The datasets generated and supporting the findings of this article are obtainable from the corresponding author upon reasonable request.

Nomenclature

c = linear sinusoidal sweep rate
j = imaginary unit or matrix row index
m = number of rows of the trajectory matrix
n = discrete-time variable
p = number of columns in the trajectory matrix
A = stopband attenuation
C = diagonal matrix whose squared values, $c^2{}_i$, are numerators of SOVs
D = system dynamic matrix in ERA
E = root-mean-square error between the estimated modes and the FEM-resolved modes
H = Hankel matrix in ERA
S = diagonal matrix whose squared, $s^2{}_i$, values are denominators of SOVs
T = total chirp time during the chirp excitation
U = proper orthogonal coordinate matrix
V = proper orthogonal mode matrix
X = system trajectory matrix
$\mathcal{A}$ = discrete-time state transition matrix
$\mathcal{D}$ = temporal derivative operator
u_0 = initial state vector in ERA
w_i = scalar modal clustering measure
$\underset{\sim}{Y}_i$ = ith subband trajectory matrix
$\widehat{f}_i$ = SBD-estimated damped natural frequency of the ith mode
I_0 = zero-order modified Bessel function of the first kind
S_{jk} = cosine similarity matrix whose (j,k) nomenclature characterizes the cosine similarity between the jth and the kth smooth modes
$(\cdot)_{H0}$, $(\cdot)_{H0r}$ = the resultant SVD-decomposed matrices and their reduced forms in ERA
$(\cdot)^*$ = complex conjugation
$(\cdot)^\dagger$ = Moore–Penrose pseudo inverse
$\widehat{D}$, $\hat{P}$, $\hat{Q}$, $\widehat{p}_i$ = ERA estimated system dynamics matrix, observability matrix, controllability matrix, and poles
$h_D[n]$ = ideal discrete-time impulse response function
$h_i[n]$ = discrete-time impulse response function of the ith subband
$w[n]$ = discrete-time windowing function
$x_i, \widehat{x}_i$ = FEM mode amplitude and estimated mode amplitude of the ith mode
$H(j\omega)$, R_l, p_l = system transfer function, system residues, and system poles
BW = bandwidth of the bandpass filters
O, P, Q = observation matrix, observability matrix, and controllability matrix in ERA

Greek Symbols

α_1, α_2 = Rayleigh damping coefficients
β = ripple control parameter
ζ_i = damping ratio of the ith mode
Θ_{jk} = angular similarity matrix derived from the cosine similarity matrix $S_{\phi jk}$
λ_i = square of the ith proper orthogonal value
μ_i = the ith smooth orthogonal value
σ_i = the ith proper orthogonal value
Σ = proper orthogonal values matrix
Φ_i = ith subband smooth mode matrix
Ψ, Ψ' = the eigenvectors of the estimated system dynamics matrix in physical and observation space, respectively
ω = angular frequency

References

[1] Ewins, D. J., 2009, *Modal Testing: Theory, Practice and Application*, John Wiley & Sons, Hoboken, NJ, pp. 1–18.
[2] Felber, A. J., 1994, "Development of a Hybrid Bridge Evaluation System," Ph.D. dissertation, University of British Columbia, pp. 53–55.
[3] Schwarz, B., and Richardson, M., 2001, "Modal Parameter Estimation From Ambient Response Data," Proceedings of IMAC 19, Orlando, FL, Feb. 5–8,

Downloaded from http://asmedigitalcollection.asme.org/vibrationacoustics/article-pdf/145/1/011005/6912201/vib_145_1_011005.pdf by guest on 15 October 2024

[4] Ozdemir, A. A., and Gumussoy, S., 2017, "Transfer Function Estimation in System Identification Toolbox Via Vector Fitting," IFAC-PapersOnLine, **50**(1), pp. 6232–6237.
[5] Sen, D., Erazo, K., Nagarajaiah, S., and Sun, L., 2019, "On the Effectiveness of Principal Component Analysis for Decoupling Structural Damage and Environmental Effects in Bridge Structures," J. Sound Vib., **457**, pp. 280–298.
[6] Banan, M., and Mehdi-Pour, Y., 2007, "Detection and Assessment of Damage in 2D Structures Using Measured Modal Response," J. Sound Vib., **306**(3–5), pp. 803–817.
[7] Bendat, J., and Piersol, A., 1993, *Engineering Applications of Correlation and Spectral Analysis*, John Wiley & Sons, Hoboken, NJ, pp. 196–202.
[8] Brincker, R., Zhang, L., and Andersen, P., 2000, "Modal Identification From Ambient Responses Using Frequency Domain Decomposition," Proceedings of the 18th International Modal Analysis Conference (IMAC), Vol. 1, San Antonio, TX, Feb. 7–10, pp. 625–630.
[9] Brincker, R., Andersen, P., and Jacobsen, N.-J., 2007, "Automated Frequency Domain Decomposition for Operational Modal Analysis," Conference Proceedings: IMAC-XXIV: A Conference & Exposition on Structural Dynamics, St. Louis, MO, Jan. 30–Feb. 2, Society for Experimental Mechanics.
[10] Juang, J.-N., and Pappa, R. S., 1985, "An Eigensystem Realization Algorithm for Modal Parameter Identification and Model Reduction," J. Guid. Control Dyn., **8**(5), pp. 620–627.
[11] De Callafon, R. A., Moaveni, B., Conte, J. P., He, X., and Udd, E., 2008, "General Realization Algorithm for Modal Identification of Linear Dynamic Systems," J. Eng. Mech., **134**(9), pp. 712–722.
[12] Kerschen, G., Golinval, J.-C., Vakakis, A. F., and Bergman, L. A., 2005, "The Method of Proper Orthogonal Decomposition for Dynamical Characterization and Order Reduction of Mechanical Systems: An Overview," Nonlinear Dyn., **41**(1–3), pp. 147–169.
[13] Chelidze, D., and Zhou, W., 2006, "Smooth Orthogonal Decomposition Based Vibration Mode Identification," J. Sound Vib., **292**(3–5), pp. 461–473.
[14] Han, S., and Feeny, B., 2003, "Application of Proper Orthogonal Decomposition to Structural Vibration Analysis," Mech. Syst. Signal Process, **17**(5) pp. 989–1001.
[15] Kim, B. H., Stubbs, N., and Park, T., 2005, "A New Method to Extract Modal Parameters Using Output-Only Responses," J. Sound Vib., **282** (1–2), pp. 215–230.
[16] Holguín-Londoño, M., Cardona-Morales, O., Sierra-Alonso, E. F., Mejia-Henao, J. D., Orozco-Gutiérrez, Á., and Castellanos-Dominguez, G., 2016, "Machine Fault Detection Based on Filter Bank Similarity Features Using Acoustic and Vibration Analysis," Math. Probl. Eng., **2016**, p. 7906834.
[17] Berkooz, G., Holmes, P., and Lumley, J. L., 1993, "The Proper Orthogonal Decomposition in the Analysis of Turbulent Flows," Annu. Rev. Fluid Mech., **25**(1), pp. 539–575.
[18] Liang, Y., Lee, H., Lim, S., Lin, W., Lee, K., and Wu, C., 2002, "Proper Orthogonal Decomposition and Its Applications– Part I: Theory," J. Sound Vib., **252**(3), pp. 527–544.
[19] Golub, G. H., and Van Loan, C. F., 2013, *Matrix Computations*, JHU Press, pp. 465–467.
[20] MathWorks, Inc., 2022, "Generalized Singular Value Decomposition," https://www.mathworks.com/help/matlab/ref/gsvd.html, Accessed May 19, 2022.
[21] Feeny, B., and Farooq, U., 2008, "A Nonsymmetric State-Variable Decomposition for Modal Analysis," J. Sound Vib., **310**(4–5), pp. 792–800.
[22] Zhou, W., and Chelidze, D., 2008, "Generalized Eigenvalue Decomposition in Time Domain Modal Parameter Identification," ASME J. Vib. Acoust., **130**(1), p. 011001.
[23] Farooq, U., and Feeny, B. F., 2012, "An Experimental Investigation of State-Variable Modal Decomposition for Modal Analysis," ASME J. Vib. Acoust., **134**(2), p. 021017.
[24] Brincker, R., and Ventura, C., 2015, *Introduction to Operational Modal Analysis*, John Wiley & Sons, Hoboken, NJ, pp. 251–254.
[25] Mohanty, P., and Rixen, D. J., 2006, "Modified Era Method for Operational Modal Analysis in the Presence of Harmonic Excitations," Mech. Syst. Signal Process, **20**(1), pp. 114–130.
[26] Clough, R., and Penzien, J., 1975, *Dynamics of Structures*, McGraw-Hill, New York, p. 224.
[27] Ifeachor, E. C., and Jervis, B. W., 1993, *Digital Signal Processing: A Practical Approach*, Pearson Education Limited, pp. 349–366.
[28] Feeny, B., 2002, "On the Proper Orthogonal Modes and Normal Modes of Continuous Vibration Systems," ASME J. Vib. Acoust., **124**(1), pp. 157–160.
[29] Schwarz, B. J., and Richardson, M. H., 1999, "Experimental Modal Analysis," Proceedings of CSI Reliability Week, Orlando, FL, Oct. 4.

Downloaded from http://asmedigitalcollection.asme.org/vibrationacoustics/article-pdf/145/1/011005/6912201/vib_145_1_011005.pdf by guest on 15 October 2024